The Journal of Experimental Biology 213, 3832-3842

doi:10.1242/jeb.040790

The flow fields involved in hydrodynamic imaging by blind Mexican cave fish (*Astyanax fasciatus*). Part II: gliding parallel to a wall

Shane P. Windsor*, Stuart E. Norris, Stuart M. Cameron, Gordon D. Mallinson and John C. Montgomery

School of Biological Sciences, University of Auckland, Private Bag 92019, Auckland 1142, New Zealand

*Author for correspondence at present address: University of Oxford, Department of Zoology, Tinbergen Building, South Parks Road, Oxford OX1 3PS, UK (shane.windsor@zoo.ox.ac.uk)

Accepted 26 August 2010

SUMMARY

Blind Mexican cave fish (*Astyanax fasciatus*) are able to sense detailed information about objects by gliding alongside them and sensing changes in the flow field around their body using their lateral line sensory system. Hence the fish are able to build hydrodynamic images of their surroundings. This study measured the flow fields around blind cave fish using particle image velocimetry (PIV) as they swam parallel to a wall. Computational fluid dynamics models were also used to calculate the flow fields and the stimuli to the lateral line sensory system. Our results showed that characteristic changes in the form of the flow field occurred when the fish were within approximately 0.20 body lengths (BL) of a wall. The magnitude of these changes increased steadily as the distance between the fish and the wall was reduced. When the fish were within 0.02 BL of the wall there was a change in the form of the flow field owing to the merging of the boundary layers on the body of the fish and the wall. The stimuli to the lateral line appears to be sufficient for fish to detect walls when they are 0.10 BL away (the mean distance at which they normally swim from a wall), but insufficient for the fish to detect a wall when 0.25 BL away. This suggests that the nature of the flow fields surrounding the fish are such that hydrodynamic imaging can only be used by fish to detect surfaces at short range.

Key words: *Astyanax fasciatus*, biomechanics, computational fluid dynamics, hydrodynamic imaging, lateral line.

INTRODUCTION

Blind Mexican cave fish (*Astyanax fasciatus* Cuvier 1819) are capable of moving through complex environments without colliding with objects. The mechanism behind how these fish, which lack a visual system capable of image formation, are able to do this was initially proposed by Dijkgraaf (Dijkgraaf, 1963). As the fish swim, they displace the water they are moving through, creating a characteristic flow field around their body. As a fish approaches an object the presence of the object alters the flow field and the fish gets information about its surroundings by sensing the change in the flow field. This process has been termed 'hydrodynamic imaging' (Hassan, 1989). Fish use their mechanosensory lateral line system to detect the changes in the water flows around their body. The lateral line is composed of two types of sensory receptors; superficial neuromasts and canal neuromasts. The superficial neuromasts encode the velocity of the water flow close to the surface of the fish and the canal neuromasts encode the pressure difference between the pores of the canals in which they are located (for a review, see Coombs and Montgomery, 1999).

Studies of blind cave fish have laid the foundation for our current understanding of hydrodynamic imaging. Early studies showed that blind cave fish acquire information about objects by gliding closely alongside them. It was shown that blind cave fish have the ability to discriminate between passages with openings of different shapes (von Campenhausen et al., 1981) and between openings divided into differing width slots with vertical bars (Weissert and von Campenhausen, 1981). These experiments showed that cave fish need to be able to glide closely alongside openings in order to be able to discriminate between them. Blind cave fish appear to be able to sense highly detailed information about objects by gliding beside them, being able to detect differences in the spacing of vertical bars of less than 1.5 mm (Hassan, 1986).

Previously it had been assumed that blind cave fish rely solely on hydrodynamic information sensed by their lateral line to gain information about objects as they glide alongside them. However, recently it has been found that blind cave fish may also gain tactile information about their surroundings by touching surfaces with their extended pectoral fins (Windsor et al., 2008). The objective of this study was to measure the flow fields around blind cave fish as they swam parallel to a wall and to calculate the stimulus to their lateral line in this situation. The flow fields were measured experimentally using particle image velocimetry (PIV). Computational fluid dynamic (CFD) models were then constructed of the same situation and used to estimate the stimulus to the lateral line system. The lateral line stimuli when the fish were gliding in open water and head-on towards a wall are discussed in a companion paper (Windsor et al., 2010).

MATERIALS AND METHODS

The full details of the experimental PIV method and the CFD modelling are described in Windsor et al. (Windsor et al., 2010). Here, the methods used are briefly summarised and any aspects specific to the fish swimming parallel to a wall scenario are described.

Particle image velocimetry

Experimental PIV measurements were made of flow fields around blind cave fish swimming freely beside a vertical glass wall. The flow fields around the fish were recorded as the fish swam alongside a glass partition in an experimental tank (400 mm×300 mm×80 mm). Image sequences where the horizontal laser sheet intersected midway up the dorsal–ventral axis of a fish and in which the fish was not noticeably rolled were analysed. For the first four fish used in the experiment, the PIV camera had a field of view of

40 mm×40 mm, which gave images of the general form of the flow field around the body of the fish. The rest of the trials were conducted with a 23 mm×23 mm field of view, so as to visualise the boundary layer around the fish. Two additional cameras were also used to record the behaviour of the fish before and after they swam through the laser sheet and to record the height at which the fish swam through the laser sheet.

The PIV data was processed to extract both the velocity and pressure fields around the fish. For full details see Windsor et al. (Windsor et al., 2010; Windsor, 2008). In estimating the pressure field the velocity field was assumed to be quasi-steady, i.e. the fish as not accelerating or decelerating significantly. The stimulus to the superficial neuromasts of the lateral line was assumed to be proportional to the wall shear stress at the surface of the fish (τ_w) and the normalised skin friction coefficient (C_f) was used to compare distributions at different Reynolds numbers (*Re*). The stimulus to the canal neuromasts was assumed to be the pressure difference (ΔP) across adjacent canal pores spaced at 2% body length (BL) intervals down the body, and the difference in the pressure coefficient (ΔC_P) was used to compare distributions at different *Re*. The PIV measurements of the flow field had a number of limitations close to the body of the fish as discussed by Windsor et al. (Windsor et al., 2010). To overcome these limitations, the experimental PIV measurements were used to validate the flow fields predicted by the CFD models, which were then used to obtain a better picture of what was happening at the surface of the fish and to estimate the stimuli to the lateral line.

Computational fluid dynamics modelling

A series of 3-D CFD models were constructed using an axisymmetric body of revolution based on a NACA 0013 aerofoil to represent the shape of the fish. A 10×10×5 BL (*X*×*Y*×*Z*) domain was used, with the symmetry axis of the fish body being aligned with the *X*-axis, with the nose of the fish at the origin and the fish facing the –*X* direction. The distance of the fish body from the wall (*d*) was measured along the *Z*-axis. There were 20 nodes along each boundary face edge in the *X* and *Y* directions and 10 nodes along each edge in the *Z* direction. The –*X* face of the domain was an inlet, with a uniform inlet velocity set based on the desired *Re*. The +*X* face of the domain was set as an outlet, with zero pressure and a zero velocity gradient normal to the boundary. The +*Y*, –*Y* and +*Z* faces were set as symmetry planes. The –*Z* face was set as a no slip wall with a velocity equal to the inlet velocity. The fish geometry was set as a no slip boundary. Nodes were bunched on the –*Z* face of the domain in the area beside the fish body, to increase the mesh resolution in the volume between the body of the fish and the wall. A mesh was created around the fish with 128 nodes along the length of the fish, with 10 structured inflation layers around the fish. Nodes were bunched at the nose of the body to increase the mesh resolution in this area. The rest of the domain was filled by an unstructured Voronoi mesh. The mesh parameters used were based on a mesh refinement study conducted to establish the mesh resolution needed to accurately capture the nature of the flow field and quantify the discretisation error around the 3-D body geometry (Windsor et al., 2010). All modelling was done using the CFD code (Norris et al., 2010; Were, 1997). See Windsor et al. for full details of the CFD methodology (Windsor et al., 2010).

Models were run with the distance between the wall and the body (*d*) equal to 0.50, 0.25, 0.10, 0.05 and 0.02 BL. For the 0.02 BL model the number of nodes down the body of the fish was increased to 256 and the number of inflation layers was reduced to 6 in order to fit a sufficient number of elements in the volume between the wall and the body of the fish. The models were run at *Re* ranging from 1000 to 8000, representing the *Re* range observed in previous behavioural trials (Windsor et al., 2008).

On the head of a blind cave fish there are four lateral line canals; the supraorbital, the infraorbital, the mandibular and the preopercular. A simplified geometry was used to represent these canals in the CFD model (Fig. 1). Based on anatomical drawings (Schemmel, 1967) the canal pores were assumed to be spaced at 2% BL intervals along the canals, with a canal neuromast located midway between each pair of pores. To simplify plotting, the trunk and infraorbital canals were considered to be joined. As blind cave fish have high densities of superficial neuromasts all over their body (Teyke, 1990) it was assumed that these gave a continuous measure of shear stress over the entire body. To compare the magnitude of the lateral line stimuli to what could be detected by a blind cave fish some measure of the sensitivity of the lateral line was needed. As little is known about the sensitivity of the lateral line system in blind cave fish, data from other species was used. In ruffe (*Gemnocephalus cernuus*), the minimum threshold of the canal neuromasts is estimated to be a pressure difference of approximately 0.1 to 1.0 mPa across canal pores (van Netten, 2006). No measurement of the minimum shear stress threshold for superficial neuromasts is available. An estimate can be calculated by taking the velocity threshold of 50 μm s^{-1} (Gorner, 1963; Kroese et al., 1978) measured for the superficial neuromasts of African clawed frogs (*Xenopus laevis*) in response to a vibrating bead. If it is assumed that the flow velocity was measured at half the height of an average blind cave fish neuromast (50 μm) (Teyke, 1990), and if the effects of a frequency-dependent boundary layer are neglected, then the minimum shear stress threshold is approximately 1 mPa. This is likely to be a somewhat lower threshold than if the effects of the boundary layer were included. In the analysis of the lateral line stimuli if the calculated stimulus for a canal or superficial neuromast was less than 1 mPa then the stimulus for that neuromast was assumed to be 1 mPa. This represents the fish being unable to discriminate between stimuli below this threshold and the spontaneous activity of the neuromast.

RESULTS

General form of flow field

The PIV analyses showed systematic changes to the flow fields around blind cave fish as they glided at different distances from the wall of the tank (Fig. 2). The flow fields are described here in the frame of reference of the fish. The presence of the wall did not

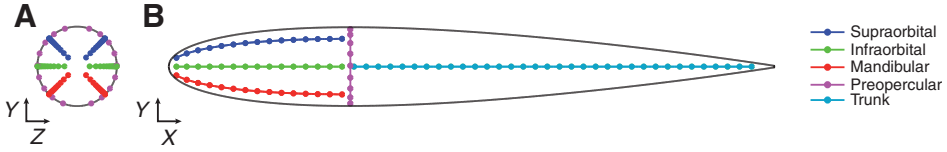

Fig. 1. Canal lateral line approximation for a 3-D axisymmetric body of revolution based on a NACA 0013 aerofoil. Canal pores are spaced 0.02 body lengths (BL) apart and are marked by circles; neuromasts are located between each adjacent pair of pores. (A) Anterior view. (B) Lateral view.

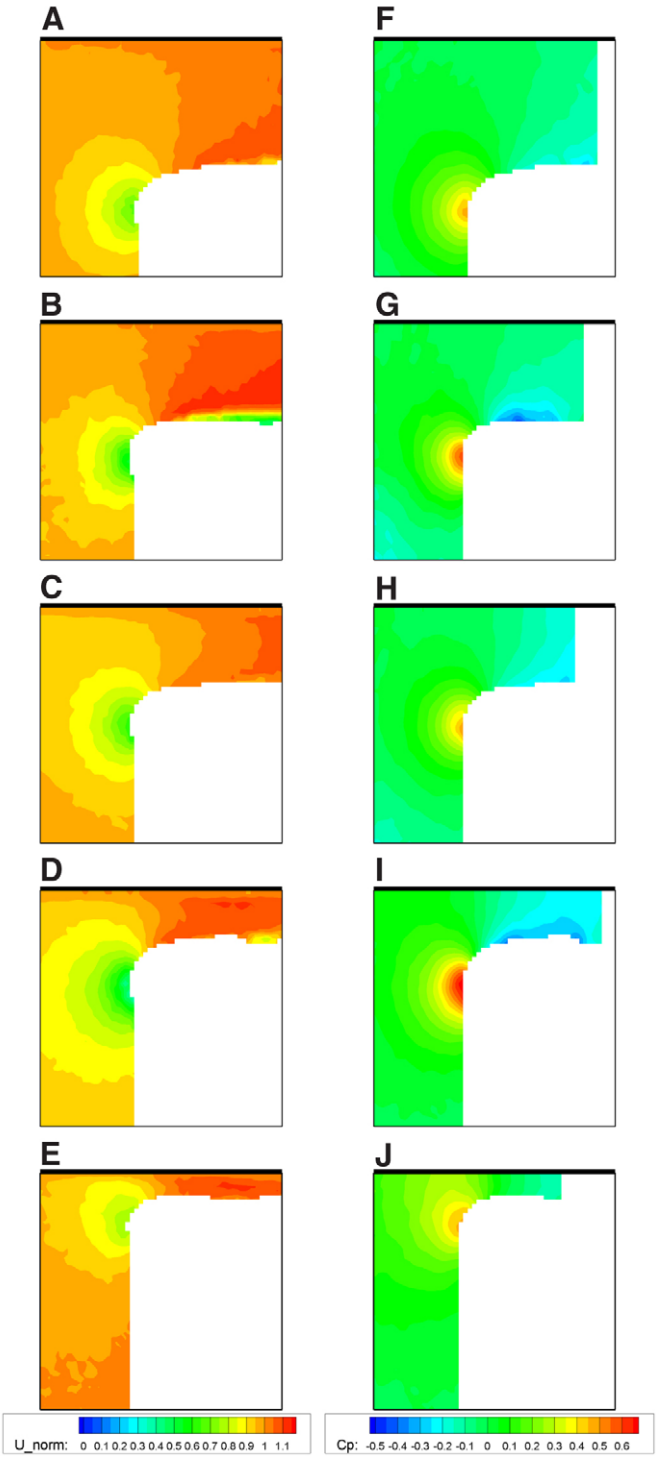

Fig. 2. Particle image velocimetry (PIV) measurements of flow fields around blind cave fish gliding parallel to a wall at different distances at a Reynolds number (*Re*) of approximately 6000. The tank wall is at the top of each image. The shadow of the fish obscures the flow field on the far side of the fish. (A–E) Normalised velocity field (U_{norm}) contours. The velocity field was normalised by dividing by the swimming velocity of the fish (U). (F–J) Normalised pressure field (C_P) contours. The boundary of the pressure field to the right of the image was moved in some cases because of the presence of the fish's pectoral fin. (A,F) d=0.20 BL. (B,G) d=0.15 BL. (C,H) d=0.11 BL. (D,I) d=0.06 BL. (E,J) d=0.02 BL.

appear to cause any noticeable change in the form of the flow fields around the fish when they were more than approximately 0.20 BL from the wall. When the fish were 0.15 BL from the wall, the velocity of the accelerated flow outside of the boundary layer, around the side of the fish increased slightly. At 0.11 BL from the wall, a distinct boundary layer had formed on the wall, which acted to slow the flow close to the wall, creating curved velocity contours. At 0.06 and 0.02 BL from the wall, the boundary layer on the wall slowed the flow close to the wall, but there was still a region of accelerated flow between the body of the fish and the wall. At the nose of the fish, the stagnation point appeared to move from the very tip of the nose around to the side of the fish facing the wall. The estimated pressure fields showed that the corresponding high pressure region moved with the stagnation point. It appeared that the low-pressure region at the side of the fish was also affected by the distance between the body and the wall, but the pattern of this change was difficult to interpret. The estimated pressure field in the region between the body and the wall was sensitive to experimental noise in the velocity measurements because of the small number of velocity vectors in this region and the close proximity of the boundaries where boundary condition assumptions had to be applied.

The PIV streak images and the CFD results both showed the same patterns in the flow field (Fig. 3). From the point of view of a stationary observer, the motion of the fish pushed fluid in front of the fish. The presence of the wall caused the flow in front of the fish, close to the wall, to move parallel to the wall, rather than radially relative to the nose of the fish, as it did on the other side of the fish. Down the sides of the fish, the fluid moved in the opposite direction to the motion of the fish, and then nearing the tail curved around to follow in the wake of the fish.

The CFD models showed the same general changes in flow pattern with changes in distance from the wall as were seen in the PIV results (Fig. 4). As the distance between the body and the wall was reduced, a boundary layer formed on the wall and the maximum velocity in the accelerated region between the body and the wall increased. When the body was 0.02 BL from the wall, there was a change in the form of the flow field. The size of the decelerated region remained relatively constant, while the region of accelerated flow between the wall and the body became very small, and the wake behind the body shifted towards the wall. In terms of the pressure distribution, as the distance between the body and the wall was reduced, the high pressure region around the stagnation point at the nose of the body expanded towards the wall, and the low pressure region increased in magnitude and moved down the body.

The presence of the wall to one side of the body meant that the flow fields were not axisymmetric about the body. The effect of the wall on the symmetry of the flow can be identified by looking at the cross section of the flow through the widest part of the body (Fig. 5). A boundary layer formed immediately around the body and outside of this there was a region of accelerated flow. As the distance between the wall and the body was reduced, the maximum velocity of the accelerated region on the wall side of the body increased. The boundary layer that formed on the wall could be seen by the sudden change in the shape of velocity contour lines where they approached the wall. As the distance between the body and the wall was reduced, the magnitude of the pressure in the region on the wall side of the body increased, and the direction of the steepest gradient of the pressure field became orientated vertically, rather than radially relative to the body.

Viscous boundary layers formed on the wall and on the surface of the body, as can be seen in the velocity profile across the gap between the wall and the widest point of the body of revolution

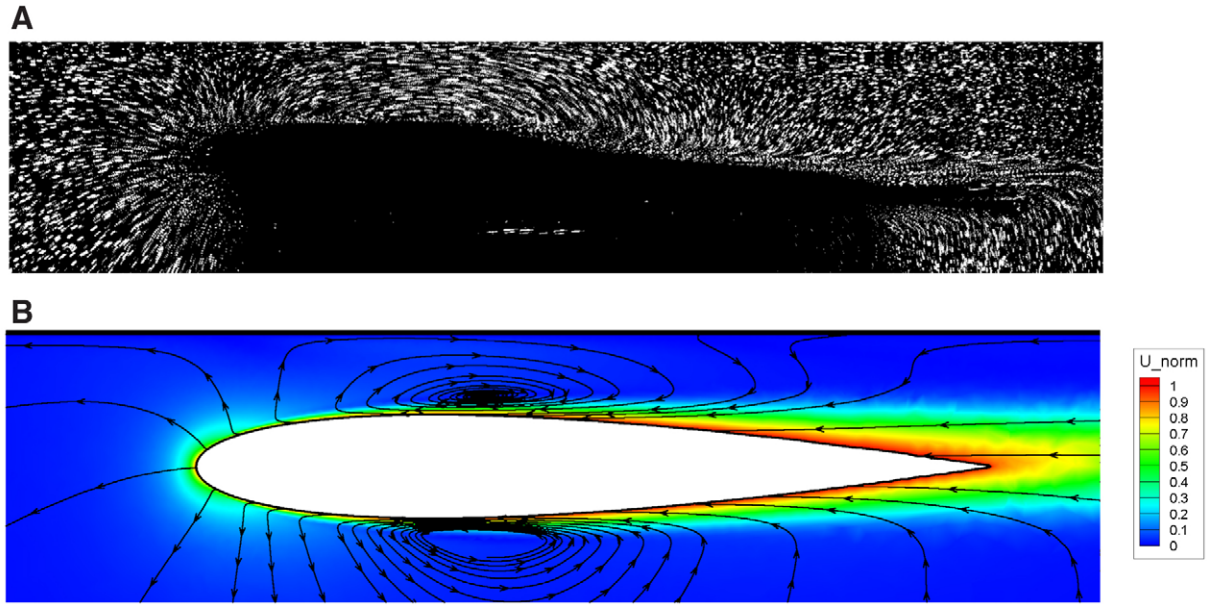

Fig. 3. Comparison of PIV and computational fluid dynamics (CFD) flow fields. (A) PIV streak image made by adding five sequential thresholded video frames of a 62 mm BL fish as it passed through the field of view at a *Re* of 16,000, 0.11 BL from the wall at the top of frame. The image was made by placing two separate streak images side by side to show the flow field over the entire body of the fish. (B) CFD solution for the flow around a 3-D body of revolution based on a NACA 0013 aerofoil, at a *Re* of 6000, 0.10 BL from the wall. Colour indicates the normalised velocity magnitude (U_{norm}) and the stream lines show the flow direction in the frame of reference of a stationary observer.

(Fig. 6). The boundary layer on the surface of the fish was created by the difference in the velocity between the fish and the free-stream velocity. The boundary layer on the wall was due to water moving between the wall and the fish at a speed greater than the free-stream velocity, because the wall can be considered to have been moving at the same speed as the free stream. The maximum velocity in the gap between the body and the wall increased as the size of the gap decreased, down to 0.05 BL. At 0.02 BL, the maximum velocity was reduced to close to the velocity of the free stream as the boundary layer on the wall and the body began to merge. The full complexity of the flow field between the body and the wall is shown by the three-dimensional (3-D) streamlines around the body (Fig. 7). The streamlines show how, when the body was close to the wall, the flow wrapped around the body, curving in three dimensions before coming back together in the wake.

The pressure distributions down the side of the body estimated from the PIV trials generally fell between two-dimensional (2-D) and 3-D CFD modelling results (Fig. 8). The PIV results showed C_P values close to the nose between the 2-D and 3-D model results, but unlike the CFD data did not have the value of 1.0 at the tip of the snout predicted by hydrodynamic theory. This is likely to be due to PIV being unable to measure the velocity of the flows very close to the body surface; the high pressure gradients normal to the tip of the snout meant that the off body pressure calculated by the PIV was not representative of the pressure at the snout. At approximately 0.10 BL down the body, the pressure predictions of the 2-D and 3-D calculations were both more positive than that captured by the PIV system. This may be due to the aerofoil shape used in the CFD calculations having a sharper nose than the fish in this region. Further down the body the pressure estimated from the PIV again fell between the 2-D and 3-D modelling results. The PIV results shown were measured over a range of *Re*, but the CFD results indicated that *Re* had a minimal effect on the normalised pressure distribution. The 2-D CFD result was obtained from a series of 2-D CFD models (Windsor, 2008) which are not presented here because the 3-D case was felt to be much more representative of the complexities of the flow around the body of a blind cave fish in this situation.

Lateral line stimuli

The stimuli to the supraorbital, infraorbital and mandibular canals on the same side of the body were very similar when the body was 0.10 BL from the wall and moving at a *Re* of 6000 (Fig. 9A,B). This was the mean distance and *Re* at which the fish swam beside a wall in behavioural trials using a very similar experimental setup (Windsor et al., 2008). The differences between the stimuli to the same canals on different sides of the body were largest near the nose. In the preopercular canal (Fig. 9C), the pressure gradients on opposite sides of the body were in opposite directions. Around the line of the preopercular canal the pressure on the body was lowest at the point closest to the wall on the ipsilateral side, and highest at the point directly opposite this on the contralateral side of the body, furthest from the wall. At these points the pressure gradient was zero as the flow was symmetric about the *XZ* plane. Away from the wall, in the open water situation, the pressure difference across all pores in the preopercular canal would be zero, with the flow being axisymmetric about the *X*-axis. The normalised lateral line stimuli did not change markedly with *Re* over the range modelled. There was a slight reduction in the normalised stimulus to the lateral line canal system for all canals with increasing *Re*, except for the preopercular canal, where the stimulus increased slightly.

Superficial neuromasts are distributed evenly and relatively densely over the body of a blind cave fish (Teyke, 1990). As such, the shear stress stimulus can be approximated as being continuously sensed over the entire body. The superficial neuromasts are directional, only sensing the wall shear stress along their axis of sensitivity. The orientation of the superficial neuromasts of the blind cave fish is not well characterised, and as such the wall shear stress

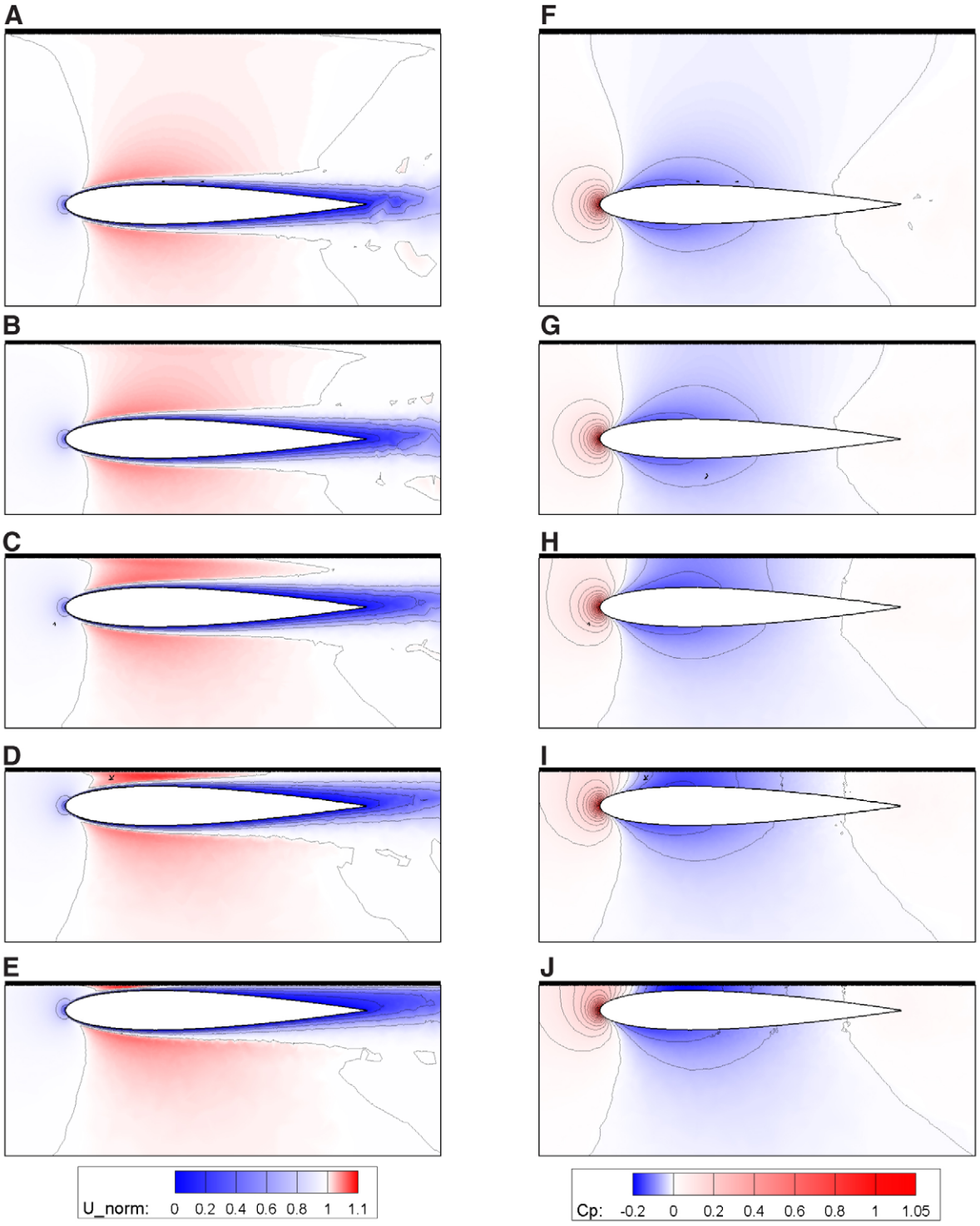

Fig. 4. Effect of the distance from the wall (d) on the flow field about a 3-D body of revolution at a Re of 6000. (A–E) Normalised velocity (U_{norm}) distribution. Colouring highlights the flow regions where the velocity was different from the inlet velocity. Velocity line contours are spaced at 0.2 intervals. (F–J) Normalised pressure (C_P) distribution. Colouring highlights the flow regions where the pressure was different from zero. C_P contour lines are spaced at 0.05 intervals. (A,F) d=0.50 BL. (B,G) d=0.25 BL. (C,H) d=0.10 BL. (D,I) d=0.05 BL. (E,J) d=0.02 BL.

shown here is the directionless total wall shear stress magnitude at each point on the surface of the body. When broken down into its individual components, the shear stresses circumferential to the body were mostly insignificant in comparison with the magnitude of the axial shear stresses, except in the area immediately around the nose of the fish.

Fish need to sense the change in the flow field around their bodies in order to gain information about their surroundings. There are a number of possible ways fish could do this. The first considered here is to sense the change in the flow field in comparison with when the fish is in open water. This can be calculated by subtracting the stimuli calculated in the open water CFD models (Windsor et

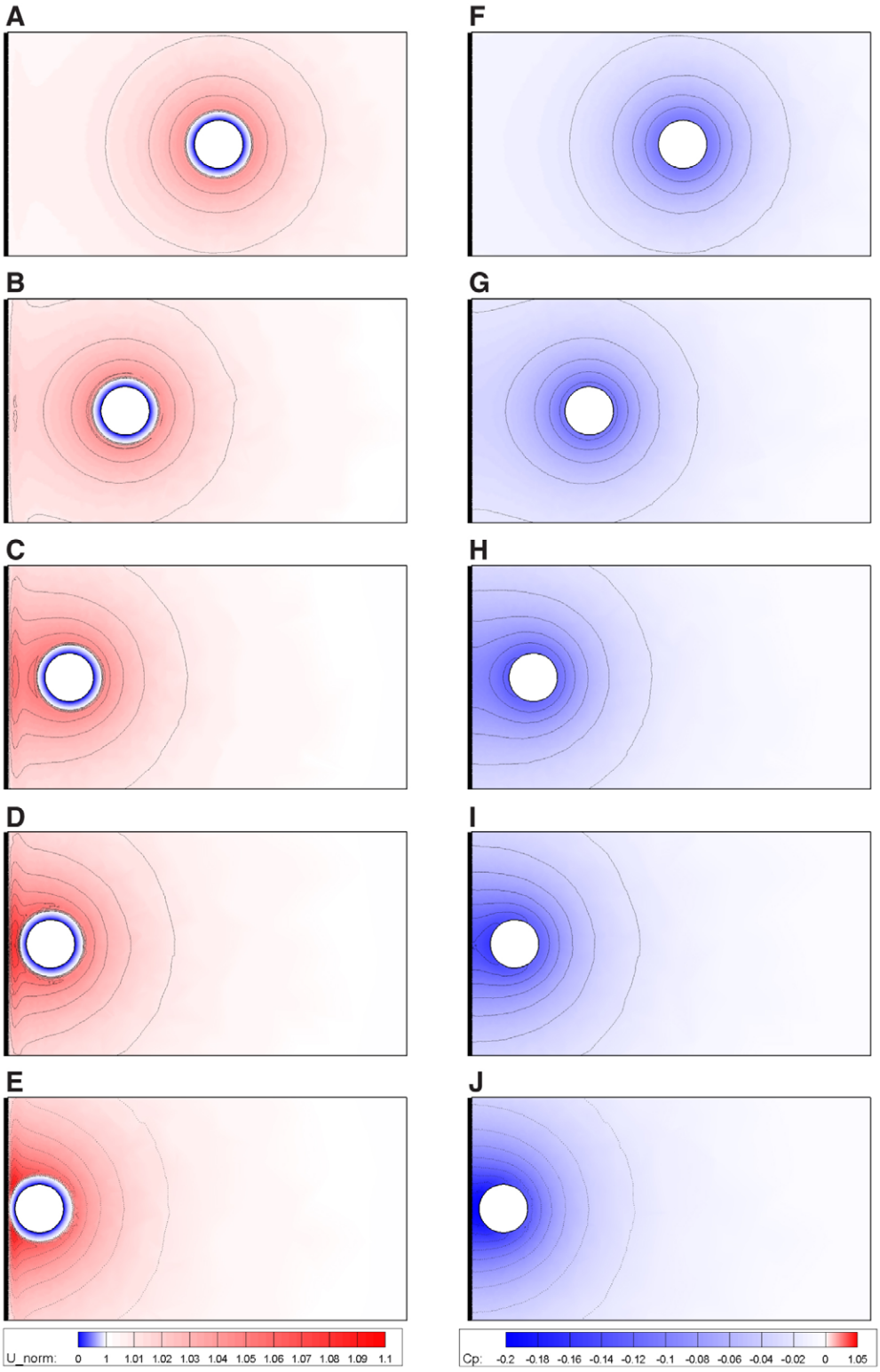

Fig. 5. Effect of the distance from the wall (d) on the flow field about a 3-D body of revolution at a *Re* of 6000, shown through a cross-section of the flow through the widest part of the body. (A–E) Normalised velocity (U_{norm}) distribution. Colouring highlights the flow regions where the velocity was different from the inlet velocity. Velocity line contours are spaced at 0.01 intervals from 1 to 1.10. (F–J) Normalised pressure (C_P) distribution. Colouring highlights the flow regions where the pressure was different from zero. C_P contour lines are spaced at 0.02 intervals from –0.2 to 0. (A,F) d=0.50 BL. (B,G) d=0.25 BL. (C,H) d=0.10 BL. (D,I) d=0.05 BL. (E,J) d=0.02 BL.

al., 2010), at the same *Re*, from that calculated in the parallel CFD models. Examining the changes in the pressure and shear distributions on the body of the fish, it is clear that the largest changes occurred at the head of the fish, on the ipsilateral side of the body (Fig. 10). These changes increased in magnitude as the distance between the body and the wall decreased. The pressure on the body

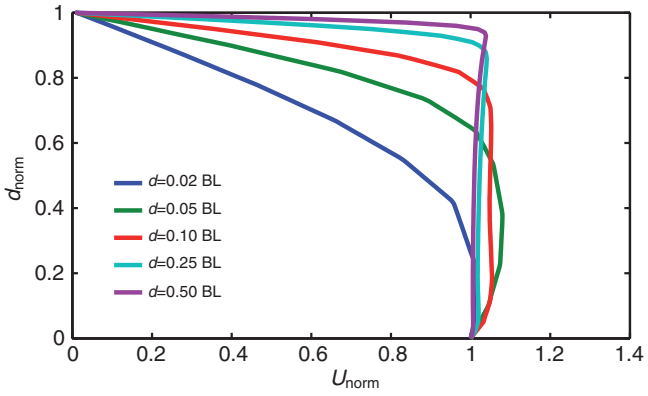

Fig. 6. Normalised x velocity (U_{norm}) across the gap between the wall and closest point on the 3-D body of revolution. The normalised distance across the gap (d_{norm}) is shown on the Y-axis with the wall at 0 and the surface of the body at 1.

increased on the side of the nose, and decreased around the widest point of the body closest to the wall. The shear stresses increased around the head of the fish and decreased near the tail.

In terms of the stimulus to the lateral line, the change in the stimuli to the different canals with distance from the wall in comparison to when gliding in open water is shown in Fig. 11. The changes in the pressure difference at the pores closest to the nose and down the side of the head are clearly evident, as is the change in the form of the flow field when 0.02 BL from the wall.

A second possible way for the fish to sense changes in the flow field is to compare the stimuli on the two sides of its body. The differences measured in this way were very similar to those measured by comparing the change in the flow relative to the open water situation, as the flow on the contralateral side of the body was generally not strongly affected by the presence of the wall. An exception to this occurred at the nose of the fish when 0.02 BL from the wall. Here, the sign of the change in the pressure difference was of the opposite sense to that found by comparing the flow to the open water case.

Rather than being sensitive to the absolute difference between a stimulus and a reference stimulus (e.g. the open water stimulus or the stimulus on the other side of the body), the fish may be sensing the relative difference between the current stimulus and the reference stimulus. Mathematically, this is done by dividing the difference between the current stimulus and the reference stimulus by the reference stimulus. This approach highlights regions where the

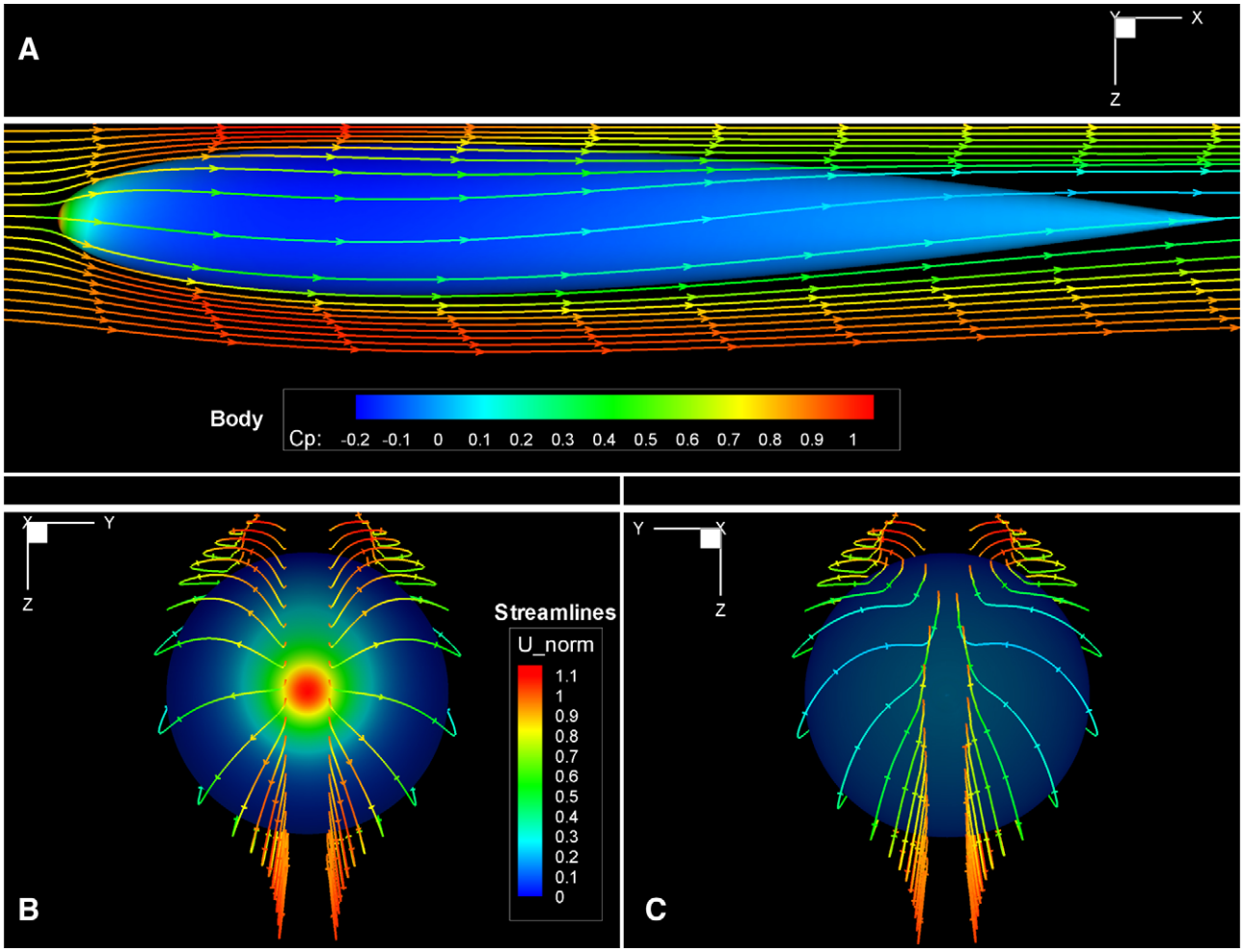

Fig. 7. Flow field around a 3-D body of revolution at a *Re* of 6000, 0.02 BL from the wall. The streamline colour represents the normalised velocity (U_{norm}). The colouring of the body represents the normalised pressure (C_P) on the body. (A) Dorsal view of body. (B) Anterior view of body. (C) Posterior view of body.

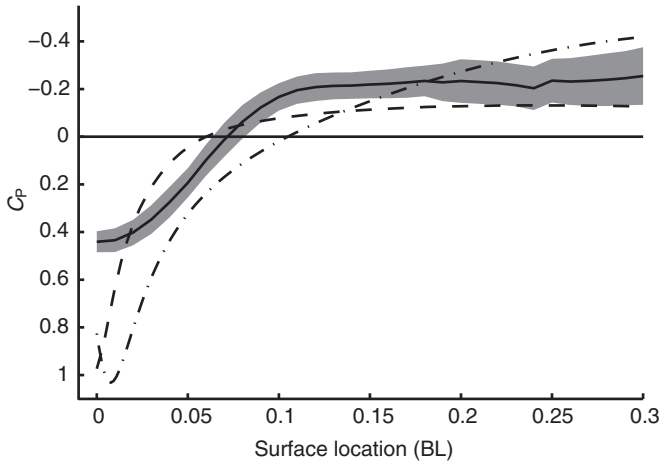

Fig. 8. PIV and CFD normalised pressure distributions on the ipsilateral side (closest to the wall) of the body at 0.10 BL from the wall. The solid black line is the mean of 9 PIV passes, with the 95% confidence intervals shown by the grey shading. PIV pressure fields were measured over a range of *Re* from 2000 to 16,000. The dashed line is the normalised pressure distribution on the NACA 0013 3-D body as calculated in the CFD model, the dot-dash line is for the 2-D fish shape; both are at a *Re* of 1000. Note that the C_P distribution is plotted with the *Y*-axis inverted in the aerodynamic convention. All distributions are only shown for the first 0.3 BL of the fish, as the PIV measurements further down the body were obscured by the pectoral fin.

reference stimulus is close to zero and then changes significantly. Alternatively, focusing on the absolute change in the stimulus tends to highlight changes in regions where the reference stimulus is large, such as around the nose of the fish. The different ways to measure the change in the stimuli to the lateral line can be compared by looking at the maximum changes measured in each way. The greatest absolute change in pressure difference occurred 0.02 BL along the infraorbital canal, with the greatest relative change in pressure difference occurring 0.18 BL along the same canal where the pressure difference in open water was very close to zero. The changes in the manibular and supraorbital canals were similar but of a slightly smaller magnitude. The stimuli to the preopercular canal were quite differently from that of the other canals on the head of the fish. The maximum changes in the preopercular canal occurred at either end of the canal, on the dorsal and ventral sides of the body and were equal and opposite. For the shear stimuli the greatest absolute change, excluding that at the very tip of the nose, occurred 0.18 BL down the body, with the greatest relative change occurring at 0.24 BL down the body, on the mid line of the ipsilateral side of the fish. The stimuli at these locations when the fish was 0.10 BL from the wall and moving at a *Re* of 6000 are compared in Table 1. At 0.25 BL from the wall, the changes in lateral line stimuli were very small. The maximum absolute change in canal stimuli occurred 0.02 BL down the infraorbital canal (ΔC_P=0.0056), which corresponded to a relative change in stimuli of 0.017. Away from the region immediately around the nose of the fish, the changes in lateral line stimuli were the same order of magnitude as the estimated threshold of the lateral line in still water (see Materials and methods).

DISCUSSION

Changes in the flow field

Experimental PIV and CFD modelling showed that, when a fish was gliding parallel to a wall, characteristic changes occurred in the flow field around the fish as the distance between the wall and the fish was reduced (Figs 2, 4 and 5). The stagnation point at the

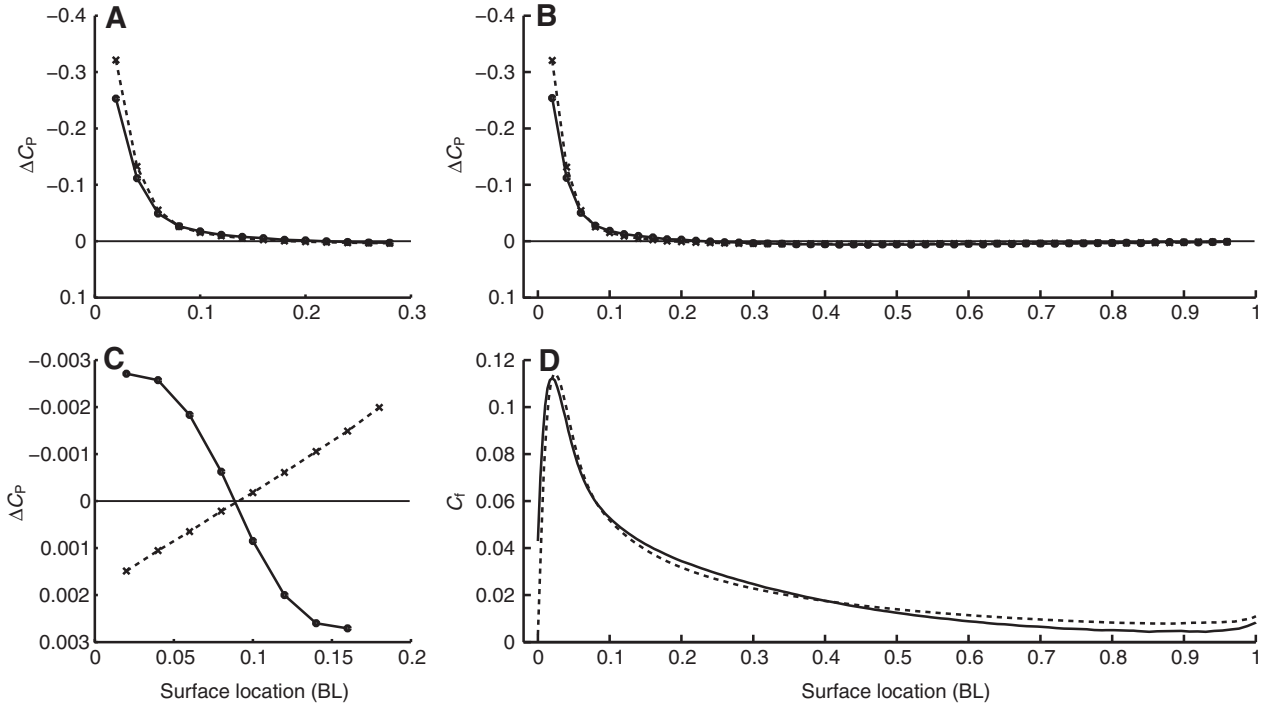

Fig. 9. Normalised pressure differences across pores of the lateral line canals on different sides of the 3-D body of revolution at a *Re* of 6000, 0.10 BL from the wall. Stimuli to the ipsilateral side (closest to the wall) are shown with solid lines. Stimuli to the contralateral side (furthest from the wall) are shown with dashed lines. (A) Supraorbital canal (the stimuli to the mandibular canal was identical because of symmetry). (B) Infraorbital canal and trunk canal. The infraorbital canal changes to the trunk canal at 0.3 BL. (C) Preopercular canal, with 0 representing the dorsal surface of the body and 0.2 the ventral surface of the body. Note the change in scale on the *Y*-axis from the other plots. (D) Superficial neuromast stimuli along the midline of the ipsilateral and contralateral surfaces of the body.

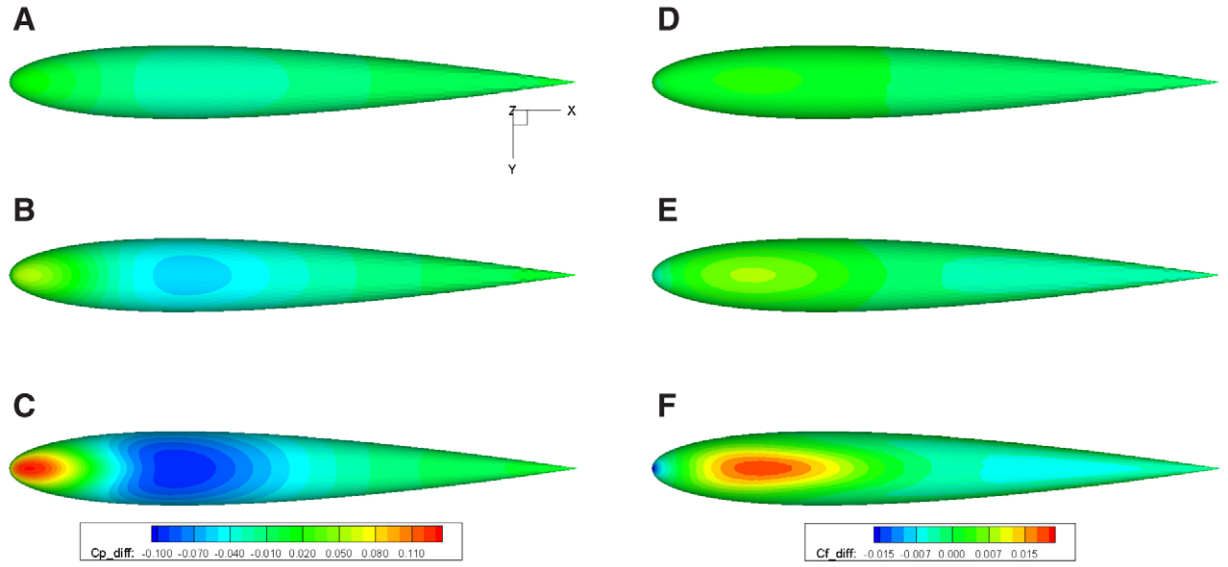

Fig. 10. Difference in the flow field on the side of a 3-D body of revolution closest to a wall at a *Re* of 6000 compared with when in open water. (A–C) Difference in normalised pressure from open water. (D–F) Difference in normalised shear stress from open water. (A,D) *d*=0.10 BL. (B,E) *d*=0.05 BL. (C,F) *d*=0.02 BL.

nose moved around to the side of the body facing the wall, and the size of the decelerated region around the stagnation point increased. The magnitude of the negative pressure region on the side of the fish towards the wall increased, and the point of minimum pressure moved down the body of the fish towards the tail. These changes are somewhat similar to what is seen at higher *Re* with aerofoils in ground-effect (Ahmed and Sharma, 2005). In ground-effect, the stagnation point moves down the side of an aerofoil closest to the ground as the aerofoil is bought closer to the ground. Similar changes in the position of the stagnation point are also seen when the angle of attack of an aerofoil in a uniform flow is increased.

When the distance between the body and the wall was decreased to 0.02 BL, there was a large change in the form of the flow field in the CFD models. It appears that this change in the flow pattern was due to the boundary layers on the body and the wall merging (Fig. 6), inhibiting the flow between the body and the wall. The

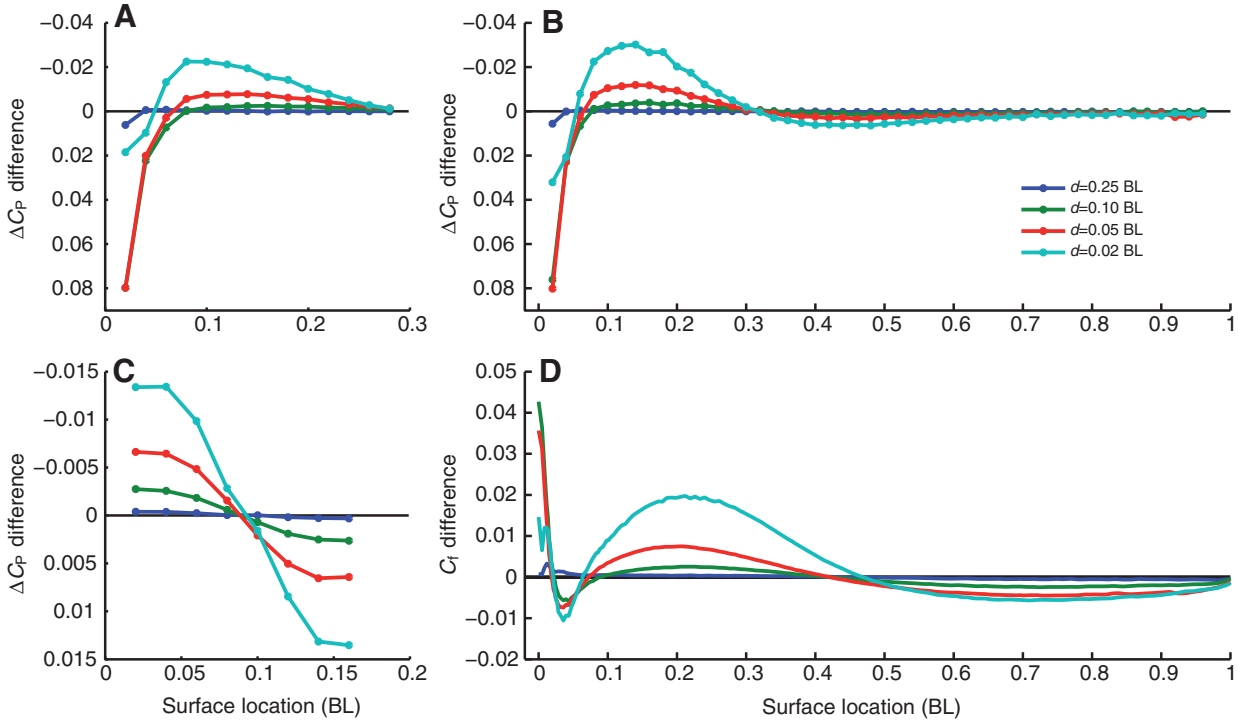

Fig. 11. Effect of distance from the wall on the difference between ipsilateral lateral line stimuli and the stimulus in open water at a *Re* of 6000. (A) Supraorbital canal (the stimuli to the mandibular canal was identical because of symmetry). (B) Infraorbital canal and trunk canal. The infraorbital canal changes to the trunk canal at 0.3 BL. (C) Preopercular canal, with 0 representing the dorsal surface of the body and 0.2 the ventral surface of the body. Note the change in scale on the *Y*-axis from the other plots. (D) Superficial neuromast stimuli along the midline of the ipsilateral surface of the body.

Table 1. Maximum stimuli differences for the three-dimensional parallel computational fluid dynamics model at a Reynolds number of 6000, 0.10 body lengths from the wall

Position	Open water	Parallel ips.	Parallel con.	Abs. difference	Rel. difference	Sides difference	Sides rel. difference
Infraorbital, 0.02 BL	–0.3301 (–3069)	–0.2540 (–2361)	–0.3205 (–2980)	0.0761 (707)	0.23	0.0665 (618)	0.21
Infraorbital, 0.18 BL	–0.0004 (–4)	–0.0034 (–32)	–0.0001* (–1)*	–0.0030 (–28)	7.80	–0.0033 (–31)	30.96
Preopercular, 0.02 BL	–0.0001* (–1)*	–0.0027 (–25)	0.0015 (14)	–0.0025 (–24)	24.20	–0.0042 (–39)	2.82
Superficial, 0.18 BL	0.0322 (299)	0.0352 (328)	0.0319 (296)	0.0030 (28)	0.09	0.0033 (31)	0.10
Superficial, 0.24 BL	0.0260 (242)	0.0288 (268)	0.0259 (240)	0.0028 (26)	0.11	0.0029 (27)	0.11

BL, body length; ips, ipsilateral; con, contralateral; Abs., absolute; Rel., relative.

Measurements for the canals are ΔC_P and for superficial neuromasts, C_f. Numbers in brackets are non-normalised measurements for a fish of the mean body length used in the particle image velocimetry experiments (44 mm) in mPa.

*A measurement below the estimated threshold of the lateral line. These measurements were replaced with the estimated sensory threshold value (1 mPa). This represents the fish being unable to discriminate between stimuli below this threshold and the spontaneous activity of the neuromast.

growth of both of these boundary layers reduced the effective gap between the wall and the fish down the entire ipsilateral side of the body. The growth of the boundary layer on the body changed the effective geometry of the body to one that was much wider down the rear half of the body.

The influence of viscosity on the stimuli to the lateral line of a small fish gliding parallel to a wall can been seen by comparing the results of the CFD model presented here with those of the potential flow models of Hassan (Hassan, 1992). Hassan's potential flow models had a similar body geometry and used a similar approximation to the layout of the lateral line canals as that used in this study. The general shape of the pressure distribution on the body of the fish was similar when the fish was 0.10 BL from the wall, but the magnitude of the stimulus was much larger in the CFD models, with the maximum difference in the C_P from open water in Hassan's model being 0.0014 and for the CFD 0.076. The stimuli distributions for the CFD models at smaller distances from the wall were of a different shape from those measured in Hassan's models; for instance Hassan's model did not show a sudden change in the shape of the C_P distribution when the body got very close to the wall. This is likely to be due to Hassan's model being inviscid and not including boundary layer effects. It is not possible to directly compare the stimuli to the superficial neuromasts between the models, as in Hassan's inviscid model the stimuli were assumed to be the velocities on the surface of the body, and in the viscous models presented here the stimuli were assumed to be the wall shear stresses. In Hassan's models, the superficial stimuli in the circumferential direction, around the body of the fish, were considerable and changed more than the axial component of the stimuli. However, this was not seen in this study, with only very small circumferential wall shear stresses being measured. Overall, the two models showed similar results in terms of the general form of the flow field when the fish was more than 0.10 BL from the wall, with the inviscid model predicting much smaller stimuli, but when the body was closer to the wall the patterns of flow differed because of the effects of viscosity. This indicates that it is important to consider the effects of viscosity at the *Re* at which most fish operate.

Sensing changes in the flow field

In order for a fish to be able to sense a wall that it is swimming parallel to it must be able to sense the change in lateral line stimuli created by the presence of the wall. For many sensory modalities, in many species (Schiffman, 1996; Teghtsoonian, 1971), it has been found that the ability to detect a difference in a stimulus is directly proportion to the magnitude of the original stimulus. This is known as Weber's law and the relative difference that can be detected is known as the Weber fraction or the just noticeable difference. No measurements of the Weber fraction for the lateral line are readily available. Based on behavioural measurements, blind cave fish swim parallel to walls at a mean distance of 0.10 BL (Windsor et al., 2008). At this distance the relative difference in lateral line stimuli at a number of different points are shown in Table 1. The absolute change in the lateral line stimuli over most of the body was well above the estimated lateral line threshold in still water and the relative change in stimuli was large in comparison with Weber fractions for other sensory modalities [approximately 0.01 to 0.08 (Teghtsoonian, 1971)]. Therefore, it is highly likely that cave fish can detect the presence of the wall when gliding 0.10 BL from the wall. The reason that the relative differences in lateral line stimuli was so much greater at 0.18 BL along the infraorbital canal and 0.02 BL along the preopercular canal than at other points on the body, is that the original stimuli in open water (or on the contralateral side of the body) was very close to zero, so even a small change in stimuli represented a very large relative change. The next largest distance modelled from the wall was 0.25 BL. At this distance the absolute change in the lateral line stimuli over almost all of the body was of the same order of magnitude as the estimated absolute lateral line threshold in still water. Only for the most anterior neuromast in each of the infraorbital, supraorbital and mandibular canals was the absolute change in canal stimuli appreciably greater than the estimated absolute threshold, and in these cases the relative change in stimuli was very small. For example, for the most anterior neuromast in the infraorbital canal the stimulus was 28 times the threshold value, but the relative change was only 0.017. In comparison to other sensory modalities this is close to the lower end of the range of measured Weber fractions. Therefore, it is possible that the fish could detect the wall at this distance, but it seems unlikely given that only three neuromasts would be sufficiently stimulated, and only then if the lateral line was very sensitive to relative changes in stimuli.

Previously it has been found that blind cave fish frequently touch surfaces with their pectoral fins while swimming (Baker and Montgomery, 1999; Windsor et al., 2008). At the mean behaviourally measured distance (0.10 BL) that fish swim parallel to a wall, the pectoral fins are long enough (0.13 BL) to give the fish tactile information about their surroundings. Therefore, it is not clear if the fish are using their sense of touch, their lateral line, or both to sense a wall beside them. The CFD modelling results indicated that at 0.10 BL from the wall the fish are likely to be able to sense the wall using their lateral line. This indicates that fish have both tactile and hydrodynamic information available to them at this

distance from the wall. However, hydrodynamic imaging alone appears to be sufficient for fish to be able to sense the presence of the wall, as blind cave fish have been commonly observed to swim parallel to walls without touching them (Windsor et al., 2008).

The changes in stimuli to the lateral line appear to be such that fish will be able to sense them whether the changes are measured relative to open water or to the other side of the body. The estimated lateral line stimuli at a number of regions on the body of the fish changed markedly irrespective of whether the change was measured in comparison with stimuli in open water, or on the opposite side of the body (Table 1). If fish compare the stimulus when they are beside a wall to that when they are in open water, then they would need to remember a template of the stimulus in open water calibrated to their swimming velocity. However, if they simply compare the stimuli on either side of their body, then this would not be necessary. The drawback with this method is that it would not work if there were objects on both sides of their body. As it stands there is not enough known about how blind cave fish process the stimuli from their lateral line to be able to say which, if either, of these methods is the more likely to be used.

The parallel and head-on cases [presented in Windsor et al. (Windsor et al., 2010)] both showed that the stimuli to the lateral line decreased rapidly the further a fish was from a surface. It appears that the nature of the flow field is such that the changes in lateral line stimuli are sufficient for fish to detect surfaces only when they are relatively close to them. The field created by the movement of the fish did not extend far in front of, or to the side of the fish, and as such this limited the range of hydrodynamic imaging. In comparison, the lateral line can be used to detect objects at larger distances (on the order of 2 BL) if sensing a flow generated externally, for example, sensing the movements of prey (Coombs and Janssen, 1990) or the interactions of a stationary object with an environmental flow (Liao, 2006).

This study measured the flow fields around gliding blind cave fish. Our results clearly showed that there is a wealth of information available in the flow fields for fish to be able to sense nearby objects. What use fish are able to make of this information depends on exactly how the stimuli to the lateral line are processed in the central nervous system and what features of the flow field are extracted. Given the current limited level of understanding, there is a clear need for further studies into the sensory processing behind hydrodynamic imaging.

LIST OF SYMBOLS AND ABBREVIATIONS

BL	body length
CFD	computational fluid dynamics
C_f	skin friction coefficient
C_P	coefficient of pressure
d	distance of the fish body from the wall
P	pressure field
PIV	particle image velocimetry
Re	Reynolds number
U_{norm}	normalised velocity field
ΔC_P	normalised pressure difference across canal pores
ΔP	pressure difference

REFERENCES

Ahmed, M. R. and Sharma, S. D. (2005). An investigation on the aerodynamics of a symmetrical airfoil in ground effect. *Exp. Therm. Fluid Sci.* **29**, 633-647.

Baker, C. F. and Montgomery, J. C. (1999). The sensory basis of rheotaxis in the blind Mexican cave fish, *Astyanax fasciatus*. *J. Comp. Physiol. A* **184**, 519-527.

Coombs, S. and Janssen, J. (1990). Behavioral and neurophysiological assessment of lateral line sensitivity in the mottled sculpin, *Cottus bairdi*. *J. Comp. Physiol. A* **167**, 557-567.

Coombs, S. and Montgomery, J. C. (1999). The enigmatic lateral line system. In *Comparative Hearing: Fish and Amphibians* (ed. R. R. Fay and A. N. Popper), pp. 319-362. New York: Springer-Verlag.

Dijkgraaf, S. (1963). Functioning and significance of lateral-line organs. *Biol. Rev. Camb. Philos. Soc.* **38**, 51-105.

Gorner, P. (1963). Untersuchungen zur morphologie und elektrophysiologie des seitenlinienorgans vom krallenfrosch (*Xenopus laevis* Daudin). *Zeitschrift Fur Vergleichende Physiologie* **47**, 316-338.

Hassan, E. S. (1986). On the discrimination of spatial intervals by the blind cave fish (*Anoptichthys jordani*). *J. Comp. Physiol. A* **159**, 701-710.

Hassan, E. S. (1989). Hydrodynamic imaging of the surroundings by the lateral line of the blind cave fish *Anoptichthys jordani*. In *The Mechanosensory Lateral Line: Neurobiology and Evolution* (ed. S. Coombs, P. Gorner and H. Munz), pp. 217-228. New York: Springer-Verlag.

Hassan, E. S. (1992). Mathematical-description of the stimuli to the lateral line system of fish derived from a 3-dimensional flow field analysis: II. The case of gliding alongside or above a plane surface. *Biol. Cybern.* **66**, 453-461.

Kroese, A. B. A., Vanderzalm, J. M. and Vandenbercken, J. (1978). Frequency-response of lateral-line organ of *Xenopus laevis*. *Pflugers Arch. Eur. J. Physiol.* **375**, 167-175.

Liao, J. C. (2006). The role of the lateral line and vision on body kinematics and hydrodynamic preference of rainbow trout in turbulent flow. *J. Exp. Biol.* **209**, 4077-4090.

Norris, S. E., Were, C. J., Richards, P. J. and Mallinson, G. D. (2010). A Voronoi based ALE solver for the calculation of incompressible flow on deforming unstructured meshes. *Int. J. Numer. Meth. Fluid.* Epub ahead of print.

Schemmel, C. (1967). Vergleichende Untersuchungen an den Hautsinnesorganen ober- und unterirdisch lebender Astyanax formen. *Zeitschrift fur Morphologie der Tiere* **61**, 255-316.

Schiffman, H. R. (1996). *Sensation and Perception: An Integrated Approach.* New York: Wiley.

Teghtsoonian, R. (1971). On the exponents in Stevens' law and the constant in Ekman's law. *Psychol. Rev.* **78**, 71-80.

Teyke, T. (1990). Morphological differences in neuromasts of the blind cave fish *Astyanax hubbsi* and the sighted river fish *Astyanax mexicanus*. *Brain Behav. Evol.* **35**, 23-30.

van Netten, S. M. (2006). Hydrodynamic detection by cupulae in a lateral line canal: functional relations between physics and physiology. *Biol. Cybern.* **94**, 67-85.

von Campenhausen, C., Riess, I. and Weissert, R. (1981). Detection of stationary objects by the blind cave fish *Anoptichthys jordani* (Characidae). *J. Comp. Physiol. A* **143**, 369-374.

Weissert, R. and von Campenhausen, C. (1981). Discrimination between stationary objects by the blind cave fish *Anoptichthys jordani* (Characidae). *J. Comp. Physiol. A* **143**, 375-381.

Were, C. J. (1997). *The Free-ALE Method for Unsteady Incompressible Flow in Deforming Geometries*. PhD Thesis. University of Auckland.

Windsor, S. P. (2008). *Hydrodynamic Imaging by Blind Mexican Cave Fish*. PhD Thesis. University of Auckland.

Windsor, S. P., Tan, D. and Montgomery, J. C. (2008). Swimming kinematics and hydrodynamic imaging in the blind Mexican cave fish (*Astyanax fasciatus*). *J. Exp. Biol.* **211**, 2950-2959.

Windsor, S. P., Norris, S. E., Cameron, S. M., Mallinson, G. D. and Montgomery, J. C. (2010). The flow fields involved in hydrodynamic imaging by blind Mexican cave fish (*Astyanax fasciatus*). Part I: open water and heading towards a wall. *J. Exp. Biol.* **213**, 3819-3831.